

Rapid emergence of life shown by discovery of 3,700-million-year-old microbial structures

Allen P. Nutman^{1,2}, Vickie C. Bennett³, Clark R. L. Friend⁴, Martin J. Van Kranendonk^{2,5,6} & Allan R. Chivas¹

Biological activity is a major factor in Earth's chemical cycles, including facilitating CO₂ sequestration and providing climate feedbacks. Thus a key question in Earth's evolution is when did life arise and impact hydrosphere–atmosphere–lithosphere chemical cycles? Until now, evidence for the oldest life on Earth focused on debated stable isotopic signatures of 3,800–3,700 million year (Myr)-old metamorphosed sedimentary rocks and minerals^{1,2} from the Isua supracrustal belt (ISB), southwest Greenland³. Here we report evidence for ancient life from a newly exposed outcrop of 3,700-Myr-old metacarbonate rocks in the ISB that contain 1–4-cm-high stromatolites—macroscopically layered structures produced by microbial communities. The ISB stromatolites grew in a shallow marine environment, as indicated by seawater-like rare-earth element plus yttrium trace element signatures of the metacarbonates, and by interlayered detrital sedimentary rocks with cross-lamination and storm-wave generated breccias. The ISB stromatolites predate by 220 Myr the previous most convincing and generally accepted multidisciplinary evidence for oldest life remains in the 3,480-Myr-old Dresser Formation of the Pilbara Craton, Australia^{4,5}. The presence of the ISB stromatolites demonstrates the establishment of shallow marine carbonate production with biotic CO₂ sequestration by 3,700 million years ago (Ma), near the start of Earth's sedimentary record. A sophistication of life by 3,700 Ma is in accord with genetic molecular clock studies placing life's origin in the Hadean eon (>4,000 Ma)⁶.

Stromatolites are broadly defined as sedimentary structures that are produced by microorganism communities through trapping and binding of sediment, and/or precipitation of carbonate⁷. Stromatolites are the most persistent evidence of life in Earth history, and are known from the present (for example, Shark Bay, Western Australia) to 3,480 Ma in the rock record^{4,5}.

Little deformed and weakly metamorphosed 3,480–3,350 Ma sedimentary rocks from the East Pilbara Terrane of the Pilbara Craton (Western Australia) contain the oldest convincing evidence for life on Earth in the form of domical and coniform stromatolites^{5,8}. In these cases, a biological origin for stromatolites is supported by morphology⁸, stable isotope signatures⁹, seawater-like trace element signatures of the dolomitic host rocks¹⁰ and the presence of microfossils¹¹. Early life environments in the Pilbara Craton included shallow marine and emergent sedimentary settings, as well as thermal springs. This variety of environments, combined with a diversity of stromatolite forms within individual units, indicates that by 3,480 Ma the biosphere was already diverse, and thus life must have originated significantly earlier¹².

The search for even earlier life is confounded by the scarcity of Eoarchaean (>3,600 Ma) and Hadean (>4,000 Ma) rocks and the strong deformation and high grade metamorphism (500–750 °C) that affected them. In most localities this has eliminated primary features within these rocks ('primary' here means structures pertaining to the

formation of the protolith, before superimposed metamorphism)³. This is a particular problem in the search for signs of early life in carbonate rocks, owing to the propensity of carbonates to undergo ductile deformation and recrystallize as marble during metamorphism and orogeny. Consequently, the search for evidence of life in Eoarchaean rocks has focused on chemical signatures, such as the isotopic compositions of carbon (as graphite) and iron from metasedimentary rocks, but the origin of these signatures is not unique and their significance as evidence of ancient life remains debated^{2,13,14,15}. Most isotopic searches for the oldest evidence of life have targeted the ISB of southwest Greenland, because it contains by far the largest areal extent of diverse Eoarchaean metasedimentary rocks with rare, small areas of low deformation in which primary sedimentary structures are preserved¹⁶.

This contribution presents the discovery of ~3,700-Myr-old structures (Fig. 1) interpreted as stromatolites in an ISB outcrop of dolomitic rocks, newly exposed by melting of a perennial snow patch. The stromatolite discovery locality (Extended Data Fig. 1) is within the hinge of an anticline cored by 3,709 ± 9-Myr-old andesitic metavolcanic rocks with locally preserved pillow structures and a maximum metamorphic temperature of ~550 °C^{17,18}. The pillowed metavolcanic rocks are overlain by bedded dolomite-rich metasedimentary rocks and in turn, by interlayered quartzites and metamorphosed banded iron formation that contain rare, small, high Th/U oscillatory-zoned volcano-sedimentary zircons with ages of 3,699 ± 12 and 3,691 ± 6 Myr^{3,18}. The term 'dolomite' is used here for compositions ranging from ferroan dolomite to magnesian ankerite.

Most ISB metadolomitic rocks are strongly deformed with quartz + tremolite + calcite ± phlogopite ± muscovite or tremolite + dolomite + calcite ± phlogopite ± muscovite mineral assemblages (Extended Data Fig. 2a). However, within the ~30 m by ~70 m low-strain lacuna discovery locality, there are domains where a CO₂-rich fluid phase was maintained during 550–500 °C metamorphism, meaning that quartz and dolomite were still in equilibrium and did not react to form tremolite (Fig. 2a; Extended Data Fig. 2b). It is this absence of reaction between dolomite and quartz that aided the preservation of the fine-scale primary structures in these rocks.

At two outcrops in the low strain area are several beds with distinct, 1–4 cm high, coniform and apparently low-amplitude domical stromatolites interbedded with sedimentary rocks in which several types of depositional structures are displayed, pointing to shallow water conditions are locally preserved. At site 'A' near the edge of the low-strain lacuna, coniform to domical stromatolites occur in three beds (Fig. 1a, b; see Extended Data Figs 2c, 3 and 4). The outcrop preserves these structures only in cross section, and their profiles are triangular to dome-shaped, the former geometry having a sharp apex at the top and a flat base that is consistent with bedding top directions in associated metasedimentary rocks (see Methods for more detailed description). The three-dimensional geometry of the stromatolites is as elongated,

¹GeoQUEST Research Centre, School of Earth & Environmental Sciences, University of Wollongong, Wollongong, New South Wales 2522, Australia. ²Australian Centre for Astrobiology, University of New South Wales, Kensington, New South Wales 2052, Australia. ³Research School of Earth Sciences, Australian National University, Canberra, Australian Capital Territory 0200, Australia.

⁴Glendale, Tiddington, Oxon, Oxford OX9 2LQ, UK. ⁵School of Biological, Earth and Environmental Sciences, University of New South Wales, Kensington, New South Wales 2052, Australia.

⁶Australian Research Council Centre of Excellence for Core to Crust Fluid Systems, School of Biological, Earth and Environmental Sciences, University of New South Wales, Kensington, New South Wales 2052, Australia.

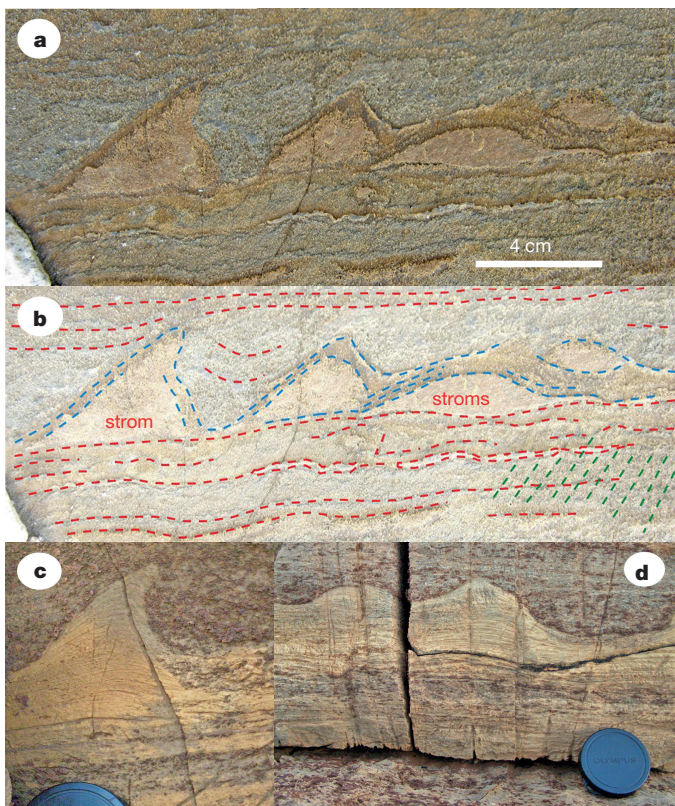


Figure 1 | ISB site A stromatolites and younger ones from Western Australia. **a**, Site A stromatolites. Image is inverted because layering is overturned in a fold. **b**, Interpretation of **a**, with isolated stromatolite (*strom*) and aggregate of stromatolites (*stoms*). Locally, lamination is preserved in the stromatolites (blue lines). Layering in the overlying sediment (red lines) onlaps onto the stromatolite sides. A weak tectonic foliation is indicated (green lines). **c**, Asymmetrical stromatolite and **d**, linked domical stromatolites from the Palaeoproterozoic²⁸ Wooly Dolomite, Western Australia. The lens cap is 4 cm in diameter. Image **c** is left-right-reversed for comparison with panels **a**, **b**.

commonly asymmetrical cones or domes, as demonstrated by images of a sawn block from the outcrop (Extended Data Fig. 4). Some of the conform structures are asymmetrical, with one of their sides steeper than the other, similar to the asymmetry displayed by some better preserved stromatolites from the ~3,400-Myr-old Strelley Pool Formation and ~2,030-Myr-old Wooly Dolomite (Fig. 1c, d; for example, see ref. 12).

Amphibolite facies metamorphism has caused recrystallization of the stromatolites to 100–200 µm granoblastic aggregates of dolomite + quartz (Extended Data Fig. 3a) that mostly obscures original fine-scale growth structures. Nonetheless, on outcrop the outer margins of site A stromatolites show internal lamination that is continuous across the crests of the structures (Fig. 1a, b). Additionally, backscattered electron imaging near the crest of a structure demonstrates preservation of a millimetre-scale compositional layering parallel to the upper bounding surface of the stromatolite, despite Ostwald ripening during recrystallization giving the current granoblastic texture (Extended Data Fig. 3). Both the outcrop exposures (Fig. 1a, b) and cut surfaces of the sawn sample (Extended Data Fig. 4) show that thin, horizontal sedimentary beds onlap the dipping sides of the stromatolites in a similar fashion as documented for 3,400-Myr-old Strelley Pool Formation stromatolites and indeed stromatolites of any age¹². Significantly, Ti and K abundances, which are indicative of phlogopite content reflecting an original muddy component of the sediment, are lower by an order of magnitude in the stromatolites relative to the adjacent sediment (Extended Data Fig. 4d). This supports the theory of the stromatolites having grown by microbial activity rather than by abiogenic precipitation of mineral crusts.

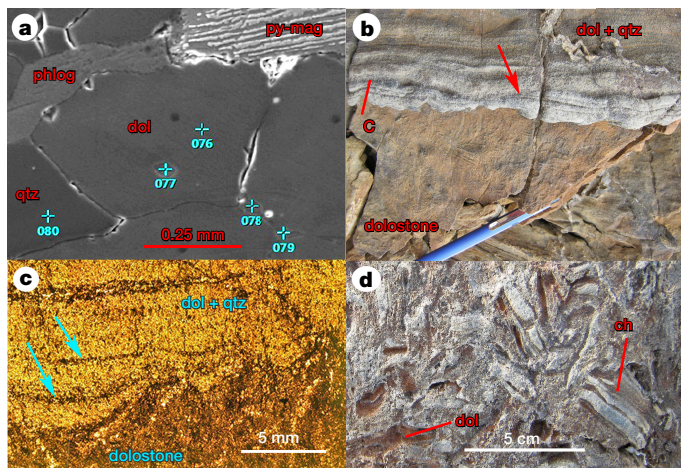


Figure 2 | ISB stromatolite mineralogical textures and site B and C occurrences. **a**, SEM image showing quartz (qtz) and dolomite (dol) equilibrium, with phlogopite (phlog) and pyrite + magnetite (py-mag). Blue crosses with numerals are energy dispersive spectra analytical sites. **b**, Site B dolostone (dolostone) has domical interface with cross-laminated dolomitic sandstone (dol + qtz; image top). The red arrow indicates erosional scouring of a layer. ‘C’ indicates the site of the thin section in **c**. Pen for scale. **c**, Photomicrograph from the domical interface, showing draping of phlogopite + dolomite layers (blue arrows) within sediment immediately above a dolostone domical structure. **d**, Site C breccia with layered chert (ch) and dolomite (dol) jumbled clasts.

At site ‘B’, lower amplitude (1 cm), more closely spaced, domical stromatolites are outlined at the top of a metadolomite unit where it is overlain by bedded, cross-laminated metasandstones (quartz + minor dolomite + phlogopite ± muscovite; Fig. 2b, c, Extended Data Fig. 2d and Extended Data Table 1). Bedding in the sedimentary rock immediately above the metadolomite is defined by draping phlogopite + dolomite laminae and contrasts sharply with the well-developed, centimetre-scale cross-stratification present in the overlying quartz-rich metasandstones that gives a way-up indicator. The cross-lamination is hummocky, with clearly developed erosional surfaces. This type of depositional structure is most widely developed where there is repeated change of current direction, such as controlled by tides. This bedding style is distinct from, and unaffected by, the underlying domical structures and represents one of the best-preserved sedimentary structures in the Isua supracrustal belt (Fig. 2b, c; Extended Data Fig. 2b).

Low-deformation lacuna site ‘C’ preserves a 30-cm-thick dolomite-rich breccia lens that is associated with dolostone (Fig. 2d). The breccia consists of randomly orientated, angular clasts of bedded quartz-rich and carbonate-rich metasedimentary rocks in a finer grained dolomite + quartz matrix. Some clasts contain abundant hyalophane (Extended Data Table 1), a barium-rich feldspar that commonly develops in metamorphosed dolomitic, marly, evaporitic rocks¹⁹. The random orientation of the clasts, combined with some showing plastic deformation, resembles tempestite breccias formed in shallow marine environments where partially lithified material is ripped up and redeposited by deepening of the wave base during storms. This shallow water setting contrasts with evidence that sedimentary rocks in other tectonic packages of the ISB formed in deeper water conditions^{2,16}. This reinforces the diverse origins of different packages of rocks in the belt¹⁸.

The barium-rich character of some layers of the dolomitic succession (up to 1 wt% BaO) now represented by halogen-rich barian phlogopite ± barian muscovite ± hyalophane (Extended Data Table 1), support periodic evaporitic conditions and the generally shallow water environment. Tempestite breccias formed by wave action require ice-free waters. This, together with the absence of glaciogenic diamictites in the ISB, indicates an equable climate at 3,700 Ma that, under the faint young Sun, was probably supported by a more CO₂- and/or CH₄-rich atmosphere^{20,21}.

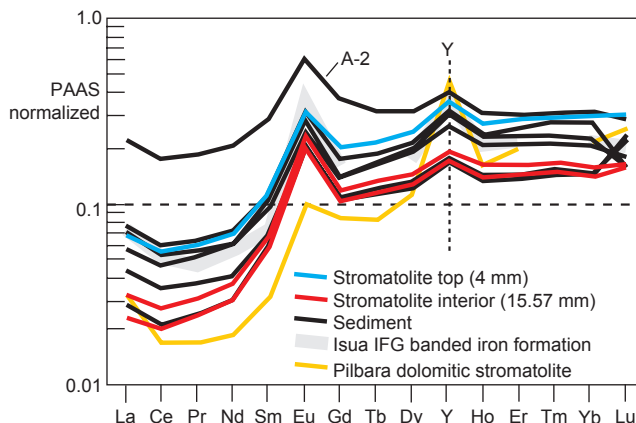


Figure 3 | PAAS-normalized (post-Archaean average shale)²⁹ rare-earth element and yttrium plot. Site A sample G12/96 Isua stromatolite dolomites and bounding sedimentary rocks are *in situ* laser-ablation inductively coupled plasma mass spectroscopy analyses from the block shown in Extended Data Fig. 4. An ~3,700-Myr-old Isua banded iron formation sample³⁰ and an East Pilbara dolomitic stromatolite¹⁰ are shown for comparison. Diagnostic of the seawater-like signature are positive yttrium (Y) and lanthanum (La) anomalies. See Methods for analytical methods and Extended Data Table 2 for analyses.

Locality A stromatolites and the bedded metadolomite interlayered with them display seawater-like rare-earth-element plus yttrium (REE+Y) signatures with diagnostic positive Y and La anomalies and low total REE contents (Fig. 3, Extended Data Table 2 and Extended Data Fig. 4). This REE+Y signature is preserved in even the most Ti-Al-rich 'marly' layer (analysis A-2 Fig. 3, Extended Data Table 2) and indicates a marine, rather than a hydrothermal, lacustrine or estuarine environment¹⁰. The lack of a discernible negative Ce anomaly (Fig. 3) is consistent with reducing conditions of deposition. The presence of accessory phlogopite ± muscovite in the bedded dolomites indicates a minor potassic input, typical of that derived from alteration, as indicated additionally by the K-enrichment in altered ISB basalts²². Significantly, stromatolitic structures are compositionally distinct from the interlayered bedded sedimentary rocks at the studied localities, as revealed by petrographic observations and geochemical traverses (Extended Data Table 2 and Extended Data Figs 2b, 3, 4c).

Stromatolitic metacarbonates have uniform carbon and oxygen isotopic values of $\delta^{13}\text{C}_{\text{VPDB}} = +1.4 \pm 0.1$ and $\delta^{18}\text{O}_{\text{VSMOW}} = +18.4 \pm 0.1$ (1σ ; Extended Data Table 3). The closed system metamorphism of these rocks, and absence of aqueous fluids leading to decarbonation reactions, suggests that primary dolomite carbon isotopic ratios would not have been significantly isotopically modified during metamorphism. The carbon isotopic compositions are consistent with precipitation from a carbonate pool from which carbon with a low $^{13}\text{C}/^{12}\text{C}$ ratio had been extracted, assuming a modern atmosphere starting isotopic composition. In modern stromatolites, this is the result of early carbonate cement precipitation in the presence of microbial communities that fixed carbon dioxide to organic matter. The Isua stromatolite-constructing communities thus show possible evidence of an autotrophic carbon-fixing metabolism. The $\delta^{18}\text{O}_{\text{VSMOW}}$ values are similar to those for stromatolitic dolomite in 3,480–3,400-Myr-old Pilbara stromatolites formed in marginal marine to evaporitic conditions²³. Given the contrast in metamorphic grade of the Pilbara and Isua samples (sub-greenschist versus low-amphibolite facies), this suggests that the Isua sample oxygen isotopic signatures reflect processes during deposition or during diagenetic cement formation shortly afterwards.

Several lines of evidence combine to indicate the biogenicity of the proposed Isua stromatolites:

(i) Sharp, steep-sided walls on Isua stromatolites are onlapped by adjacent marine dolomitic sediment, indicative of growth of the stromatolites above the sediment-water interface (compare with ref. 12).

The diversity of Isua forms matches some Palaeoarchaean stromatolites (Fig. 1).

(ii) The presence of originally low-temperature dolomite, which requires microbial activity for precipitation^{24,25}.

(iii) The stromatolite trace element compositions, including positive La anomalies, Y/Ho ratios approaching that of modern seawater, light rare-earth element depletions relative to average shale, and small positive Eu anomalies consistent with other Archaean orthochemical sedimentary rocks. This precludes formation of these structures as abiotic hydrothermal exhalites.

(iv) Internal lamination. A key feature demonstrating the biogenic origin of ancient stromatolites is a laminated growth pattern that is independent from structures formed purely by physical sedimentary processes⁷. Although recrystallized, the stromatolites preserve relicts of convex-upwards lamination (Fig. 1 and Extended Data Fig. 4) across their culminations, indicating they were not formed as dewatering structures.

Nonetheless, suggestions that some peaked or domical stromatolite-like structures could be abiogenic mineral accumulations²⁶ should be considered for the structures described here. Importantly, four significant morphological differences exist between biological stromatolites and abiogenic crusts, as also pointed out for ~3,400-Myr-old coniform stromatolites from the Pilbara Craton⁸. (i) Depending on the material used in abiogenic experiments or analogues, only either dome-shaped or peak-shaped structures form, but never the two together as observed from the Isua, and many younger, stromatolites¹². (ii) Regardless of material used, abiogenic laminae thicken in troughs, whereas in the Isua stromatolites, laminae are of minimal thickness, or are not developed in troughs. (iii) Abiogenic peaked structures do not form inclined, asymmetrical structures, whereas some Isua coniform stromatolites do. (iv) Abiogenic peaked structures form irregular projections that grow normal to the growth surface, whereas such projections are absent from Isua stromatolites. On these grounds, we rule out an abiogenic origin for Isua stromatolites.

The recognition of ~3,700-Myr-old biogenic stromatolites within Isua dolomites indicates that near the start of the preserved sedimentary record, atmospheric CO₂ was being sequestered by biological activity²⁷. The complexity and setting of the Isua stromatolites points to sophistication in life systems at 3,700 Ma, similar to that displayed by 3,480–3,400-Myr-old Pilbara stromatolites^{4,8,12}. This implies that by ~3,700 Ma life already had a considerable prehistory, and supports model organism chronology that life arose during the Hadean (>4,000 Ma)⁶. A shallow-water depositional environment is not necessary to conclude biogenicity, since deep-water microbialites and stromatolites are known. However, a shallow-water environment is supported by the associated sedimentary structures such as cross-lamination and tempestite breccias.

Online Content Methods, along with any additional Extended Data display items and Source Data, are available in the online version of the paper; references unique to these sections appear only in the online paper.

Received 11 October 2015; accepted 11 August 2016.

Published online 31 August 2016.

1. Schidlowski, M., Appel, P. W. U., Eichmann, R. & Junge, C. E. Carbon isotope geochemistry of the 3.7×10^9 -yr old Isua sediments, West Greenland: implications for the Archaean carbon and oxygen cycles. *Geochim. Cosmochim. Acta* **43**, 189–199 (1979).
2. Rosing, M. T. ^{13}C -Depleted carbon microparticles in >3700-Ma sea-floor sedimentary rocks from west greenland. *Science* **283**, 674–676 (1999).
3. Nutman, A. P. & Friend, C. R. L. New 1:20000 geological maps, synthesis and history of the Isua supracrustal belt and adjacent gneisses, Nuuk region, southern West Greenland: a glimpse of Eoarchaean crust formation and orogeny. *Precambr. Res.* **172**, 189–211 (2009).
4. Walter, M. R., Buick, R. & Dunlop, S. R. Stromatolites 3,400–3,500 Myr old from the North Pole area. *West. Aust. Nat. (Perth)* **284**, 443–445 (1980).
5. Van Kranendonk, M. J., Philippot, P., Lepot, K., Bodorkos, S. & Pirajno, F. Geological setting of Earth's oldest fossils in the c. 3.5 Ga Dresser Formation, Pilbara craton, Western Australia. *Precambr. Res.* **167**, 93–124 (2008).

6. Hedges, S. B. The origin and evolution of model organisms. *Nat. Rev. Genet.* **3**, 838–849 (2002).
7. Riding, R. in *Advances in Stromatolite Geobiology* (eds Reitner, J. et al.) (Springer-Verlag, 2011).
8. Allwood, A. C., Walter, M. R., Kamber, B. S., Marshall, C. P. & Burch, I. W. Stromatolite reef from the Early Archaean era of Australia. *Nature* **441**, 714–718 (2006).
9. Philippot, P., Van Zuilen, M., Lepot, K., Thomazo, C., Farquhar, J. & Van Kranendonk, M. J. Early Archean microorganisms preferred elemental sulfur, not sulfate. *Science* **317**, 1534–1537 (2007).
10. Van Kranendonk, M. J., Webb, G. E. & Kamber, B. S. Geological and trace element evidence for marine sedimentary environment of deposition and biogenicity of 3.45 Ga stromatolite carbonates in the Pilbara Craton, and support for a reducing Archean ocean. *Geobiology* **1**, 91–108 (2003).
11. Sugitani, K. et al. Biogenicity of morphologically diverse carbonaceous microstructures from the ca. 3400 Ma Strelley pool formation, in the Pilbara Craton, Western Australia. *Astrobiology* **10**, 899–920 (2010).
12. Van Kranendonk, M. J. in *Advances in Stromatolite Geobiology: Lecture Notes in Earth Sciences* (eds Reitner, J., Queric, N.-V. & Arp, G.) 517–534 (Springer 2011).
13. Mojzsis, S. J. et al. Evidence for life on Earth before 3,800 million years ago. *Nature* **384**, 55–59 (1996).
14. van Zuilen, M. A., Lepland, A. & Arrhenius, G. Reassessing the evidence for the earliest traces of life. *Nature* **418**, 627–630 (2002).
15. Dauphas, N. et al. Clues from Fe isotope variations on the origin of early Archean BIFs from Greenland. *Science* **306**, 2077–2080 (2004).
16. Nutman, A. P., Allaart, J. H., Bridgwater, D., Dimroth, E. & Rosing, M. T. Stratigraphic and geochemical evidence for the depositional environment of the early Archean Isua supracrustal belt, southern West Greenland. *Precambr. Res.* **25**, 365–396 (1984).
17. Rollinson, H. Metamorphic history suggested by garnet-growth chronologies in the Isua Greenstone Belt, West Greenland. *Precambr. Res.* **126**, 181–196 (2003).
18. Nutman, A. P., Bennett, V. C. & Friend, C. R. L. in *Continent Formation Through Time. The Geological Society, London, Special Publications* (eds Roberts, N. M. W., Van Kranendonk, M., Parman, S., Shirey, S. & Clift, P. D.) 113–133 (2015).
19. Feneyrol, J. et al. Evidence of evaporites in the genesis of the vanadian grossular ‘tsavorite’ deposit in Namalulul, Tanzania. *Can. Mineral.* **50**, 745–769 (2012).
20. Nutman, A. P., Bennett, V. C. & Friend, C. R. L. Waves and weathering at 3.7 Ga. Geological evidence for an equable terrestrial climate under the faint early Sun. *Aust. J. Earth Sci.* **59**, 167–176 (2012).
21. Walker, J. C. G., Hays, P. B. & Kasting, J. F. A negative feedback mechanism for the long-term stabilization of the earth’s surface temperature. *J. Geophys. Res.* **86**, 9776–9782 (1981).
22. Polat, A., Hofmann, A. W., Münker, C., Regelous, M. & Appel, P. W. U. Contrasting geochemical patterns in the 3.7–3.8 Ga pillow basalts cores and rims, Isua greenstone belt, Southwest Greenland: Implications for post-magmatic alteration. *Geochim. Cosmochim. Acta* **67**, 441–457 (2003).
23. Lindsay, J. F. et al. The problem of deep carbon – an Archean paradox. *Precambr. Res.* **143**, 1–22 (2005).
24. Vasconcelos, C., McKenzie, J. A., Bernasconi, S., Grujic, D. & Tien, A. J. Microbial mediation as a possible mechanism for natural dolomite at low temperatures. *Nature* **377**, 220–222 (1995).
25. Roberts, J. A., Bennett, P. C., González, L. A., Macpherson, G. L. & Milliken, K. L. Microbial precipitation of dolomite in methanogenic groundwater. *Geology* **32**, 277–280 (2004).
26. Grotzinger, J. P. & Rothman, D. H. An abiotic model for stromatolite morphogenesis. *Nature* **383**, 423–425 (1996).
27. Nutman, A. P., Friend, C. R. L., Bennett, V. C., Wright, D. & Norman, M. D. ≥ 3700 Ma pre-metamorphic dolomite formed by microbial mediation in the Isua supracrustal belt (W. Greenland): simple evidence for early life? *Precambr. Res.* **183**, 725–737 (2010).
28. Müller, S. G., Krapez, B., Barley, M. E. & Fletcher, I. R. Giant ore deposits of the Hamersley province related to the breakup of Paleoproterozoic Australia: New insights from *in situ* SHRIMP dating of baddelyite in mafic intrusions. *Geology* **33**, 577–580 (2005).
29. McClenann, S. M. in *Geochemistry and Mineralogy of Rare Earth Elements* (eds Lipin, B.R. & McKay, G.A.) 169–200 (Mineralogical Society of America, 1989).
30. Friend, C. R. L., Nutman, A. P., Bennett, V. C. & Norman, M. D. Seawater-like trace element signatures (REE+Y) of Eoarchean chemical sedimentary rocks from southern West Greenland, and their corruption during high grade metamorphism. *Contrib. Mineral. Petrol.* **155**, 229–246 (2008).

Acknowledgements Support provided by Australian Research Council grant DP120100273 and the GeoQuEST Research Centre, University of Wollongong (UOW). D. Wheeler, UOW, is thanked for technical assistance in carbon and oxygen isotopic analysis. L. Kinsley, Research School of Earth Sciences, Australian National University is thanked for assistance with LA-ICP-MS data acquisition. D. Adams of the Department of Earth & Planetary Sciences, Macquarie University is thanked for assistance with mineral analyses. M. Nancarrow of the Electron Microscopy Centre, UOW is thanked for assistance with SEM-imaging and mineral analyses. P. Gadd of the Australian Nuclear Science and Technology Organisation is thanked for undertaking ITRAX analyses. M.J.V.K. acknowledges support by the University of New South Wales and the Australian Research Council Centre of Excellence for Core to Crust Fluid Systems (CCFS). This is contribution 837 from the ARC Centre of Excellence for Core to Crust Fluid Systems (<http://www.ccfs.mq.edu.au>). Some analytical data were obtained using instrumentation funded by DEST Systemic Infrastructure Grants, ARC LIEF, NCRIS/Auscope industry partners and Macquarie University.

Author Contributions A.P.N. and V.C.B. undertook field work, acquisition of geochemical data and interpretation of the results. C.R.L.F. undertook fieldwork and interpretation of the results. M.J.V.K. interpreted the Isua stromatolite morphology and compared them with those from the Pilbara region of Western Australia and supplied the photographs for Fig. 1c, d. A.R.C. acquired and interpreted the stable isotope data. A.P.N. wrote the paper and all authors read and contributed comments to the work.

Author Information Reprints and permissions information is available at www.nature.com/reprints. The authors declare no competing financial interests. Readers are welcome to comment on the online version of the paper. Correspondence and requests for materials should be addressed to A.P.N. (anutman@uow.edu.au).

Reviewer Information *Nature* thanks J. Gutzmer, A. Polat, M. Tice and the other anonymous reviewer(s) for their contribution to the peer review of this work.

METHODS

No statistical methods were used to predetermine sample size. The experiments were not randomized and the investigators were not blinded to allocation during experiments and outcome assessment.

Locality A stromatolite fabrics and layering. This locality is near the edge of the low-strain lacuna and hence there is a weak foliation. This is at a high angle to the primary compositional layering (Fig. 1a, b; Extended Data Fig. 4). Related to this there is also minor incursion of hydrous fluid along grain boundaries, leading to patchy development of alteration selvedges on some dolomite grains. Extended Data Fig. 4a, b shows a montage of all four sides of a block sawn from the outcrop. The stromatolite structures have flat bases with conical tops in cross section. Although the stromatolite core areas are largely recrystallized and structureless with only vestiges of layering, the outer margins show internal lamination that is continuous across the crests of the structures (Fig. 1a, b). Subtle depositional layering and diagenetic structures in younger non-metamorphosed carbonate sedimentary rocks can be revealed by cathodoluminescence imaging. However, in the case of the Isua stromatolites, 550–500 °C metamorphic recrystallization has given a rise to a granoblastic mosaic of 100–200 µm dolomite + quartz that would have destroyed any depositional cathodoluminescence contrasts between layers. Despite this, SEM backscatter electron imaging reveals a subtle layering preserved on a millimetre scale (grey scale image analysis, with quartz and dolomite appearing with different brightness; Extended Data Fig. 3). This layering revealed by SEM imagery is the same magnitude as subtle layering preserved in younger non-metamorphosed stromatolites (for example, Fig. 1c, d). This internal lamination is important, as it precludes the structures having formed by dewatering, as this produces a central axial zone that cuts across and disrupts lamination. The sawn block (Extended Data Fig. 4a, b) shows that thin sedimentary beds onlap the sides of the stromatolites in a similar fashion as documented for 3,400-Myr-old Strelley Pool Formation stromatolites¹².

Locality B stromatolite fabrics and layering. At least one, and in some places two, thick laminations are preserved draping the observed stromatolites, and these laminations may represent internal fabrics that were present throughout the structures before pervasive recrystallization. These laminations thicken and thin along their length, indicating that they were not isopachous crusts. Some of these laminations are inclined relative to underlying bedding by up to 40°, substantially greater than the angle of repose for loose sediment. This suggests that these laminations were at least partially stabilized by cohesive microbial mats. Local peaks and crenulations are also present in the uppermost lamination with no apparent corresponding underlying relief, consistent with a biological origin but not a purely physical sedimentary origin.

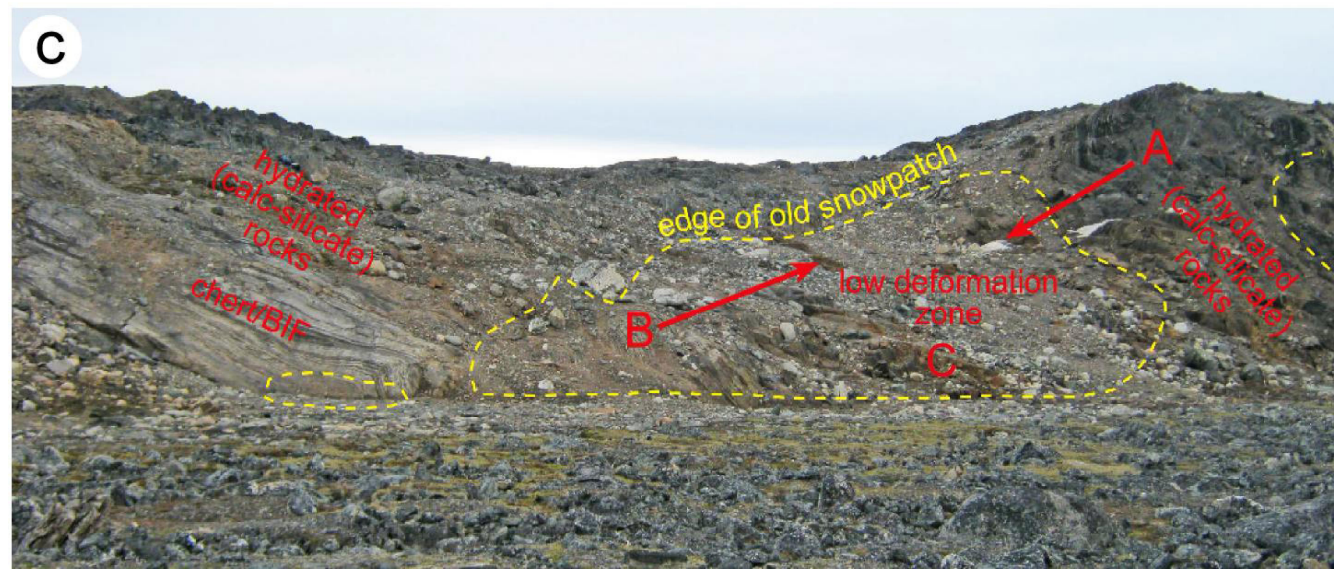
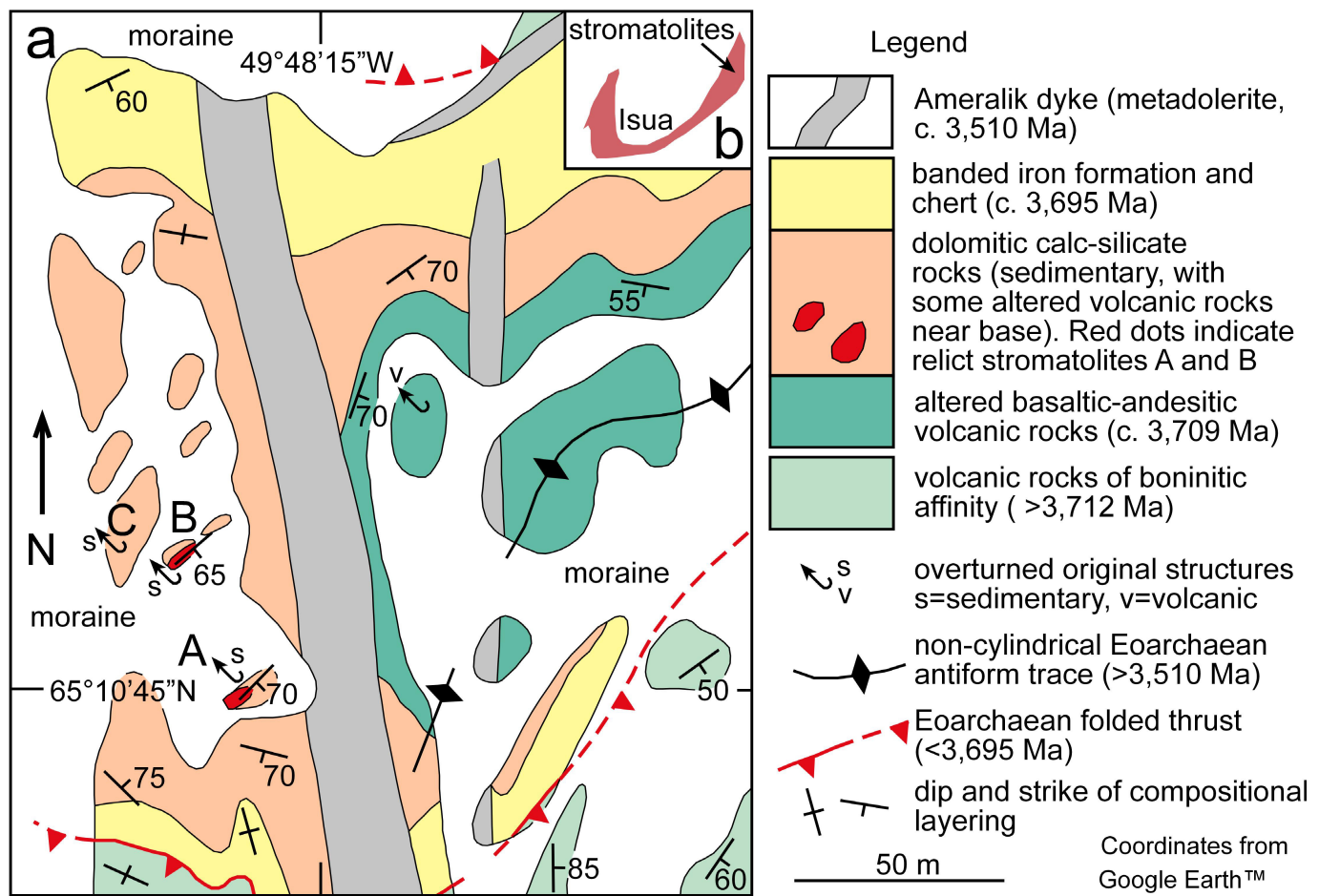
Electron probe analysis. Microprobe mineral analyses were carried out on polished thin sections using a fully automated, Cameca SX100 electron microprobe

at Macquarie University, fitted with five wavelength dispersive spectrometers (WDS). The operating conditions were: accelerating voltage 15 kV; beam current 20 nA and the beam size was focused to 20 µm for carbonates and 5 µm for other minerals.

Major and trace element analysis. For samples G11/63 and G11/72, rare-earth element concentrations were analysed commercially at the Australian Laboratory Services (ALS) at Brisbane, Australia, by inductively coupled plasma mass spectroscopy (ICP-MS) on fused glass discs. Site A sample G12/96 Isua stromatolite dolomite *in situ* trace element analyses were acquired by ICP-MS at the Australian National University using a Lambda Physik 193 nm UV excimer laser-ablation system, equipped with a dual-volume ANU HelEx chamber, coupled to a Varian 820 quadrupole ICP-MS. After laser pre-cleaning, data were acquired for 39 masses by ablation along a continuous transect across the sample perpendicular to bedding using an 800 µm by 20 µm slit moving at 10 µm per second. Laser operating conditions were 5 Hz, 24.9 mJ and 17.0 kV. Data representing the lithologic variations above, across and below the stromatolite were obtained by combining analyses into eleven segments (Extended Data Fig. 4). NIST 612 glass was used for calibration and an in-house dolomite sample was analysed as a quality control standard.

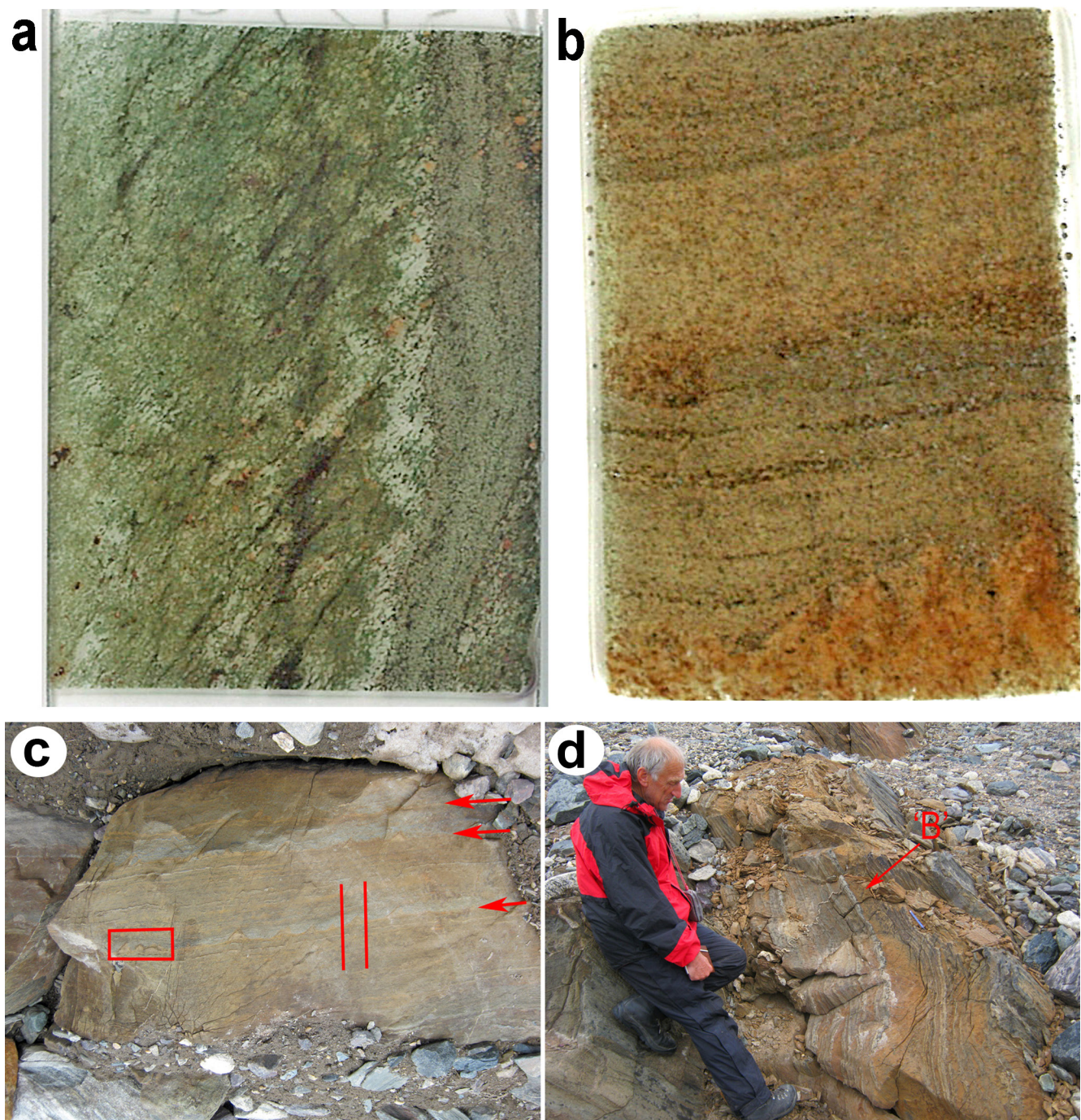
Carbon and oxygen isotopes. The ankeritic dolomite samples were reacted with 10% H₃PO₄ at 90 °C in an acid-on-individual carbonate MultiPrep system attached to a PRISM III mass spectrometer in the geochemical laboratories at the University of Wollongong. The raw δ¹⁸O values in the Table refer to the composition of the evolved CO₂ compared to that extracted from calcite from NBS-18 (δ¹⁸O_{VSMOW} = +7.19) and NBS-19 (δ¹⁸O_{VSMOW} = +28.64). The corrected values (δ¹⁸O_{VSMOWcorr}) allow for the difference (using the VSMOW scale) between 90 °C acid-liberated CO₂ from calcite and ankeritic dolomite (measured composition Ca₅₀Mg₃₀(Fe,Mn)₂₀; that is, 60% dolomite, 40% ankerite end members), for which an offset of 0.92‰ was applied³¹. The calculated δ¹⁸O value of water in equilibrium with the dolomitic samples was derived using a temperature of 525 °C and a fractionation factor at this temperature for dolomite-water of 3.6‰—extrapolation from ref. 32, as in ref. 33. Thus δ¹⁸O_{VSMOW} H₂O = 18.4 – 3.6 = +14.8‰. This value is within the range common for metamorphic water (δ¹⁸O_{VSMOW} = +3 to +20‰)³⁴.

31. Rosenbaum, J. & Sheppard, S. M. F. An isotopic study of siderites, dolomites and ankerites at high temperatures. *Geochim. Cosmochim. Acta* **50**, 1147–1150 (1986).
32. Northrop, D. A. & Clayton, R. N. Oxygen-isotope fractionations in systems containing dolomite. *J. Geol.* **74**, 174–196 (1966).
33. Friedman, I. & O’Neil, J. R. Compilation of stable isotope fractionation factors of geochemical interest, Chapter KK. Data of Geochemistry. U.S. Geological Survey Professional Paper 440-KK (1977).
34. Sheppard, S. M. F. Characterization and isotopic variations in natural waters. *Rev. Mineral.* **16**, 165–183 (1986).



Extended Data Figure 1 | Geological map and location of the described localities A, B and C. **a**, Geological map covering the described localities. The outcrops for localities A, B and C are indicated. **b**, Position of locality in the ISB. **c**, Panoramic view towards the southeast over the described

localities. In the foreground are the banded iron formation and chert outcrops in the northwest corner of the map **a**. The 15–20 m thick Ameralik dyke forms the skyline.



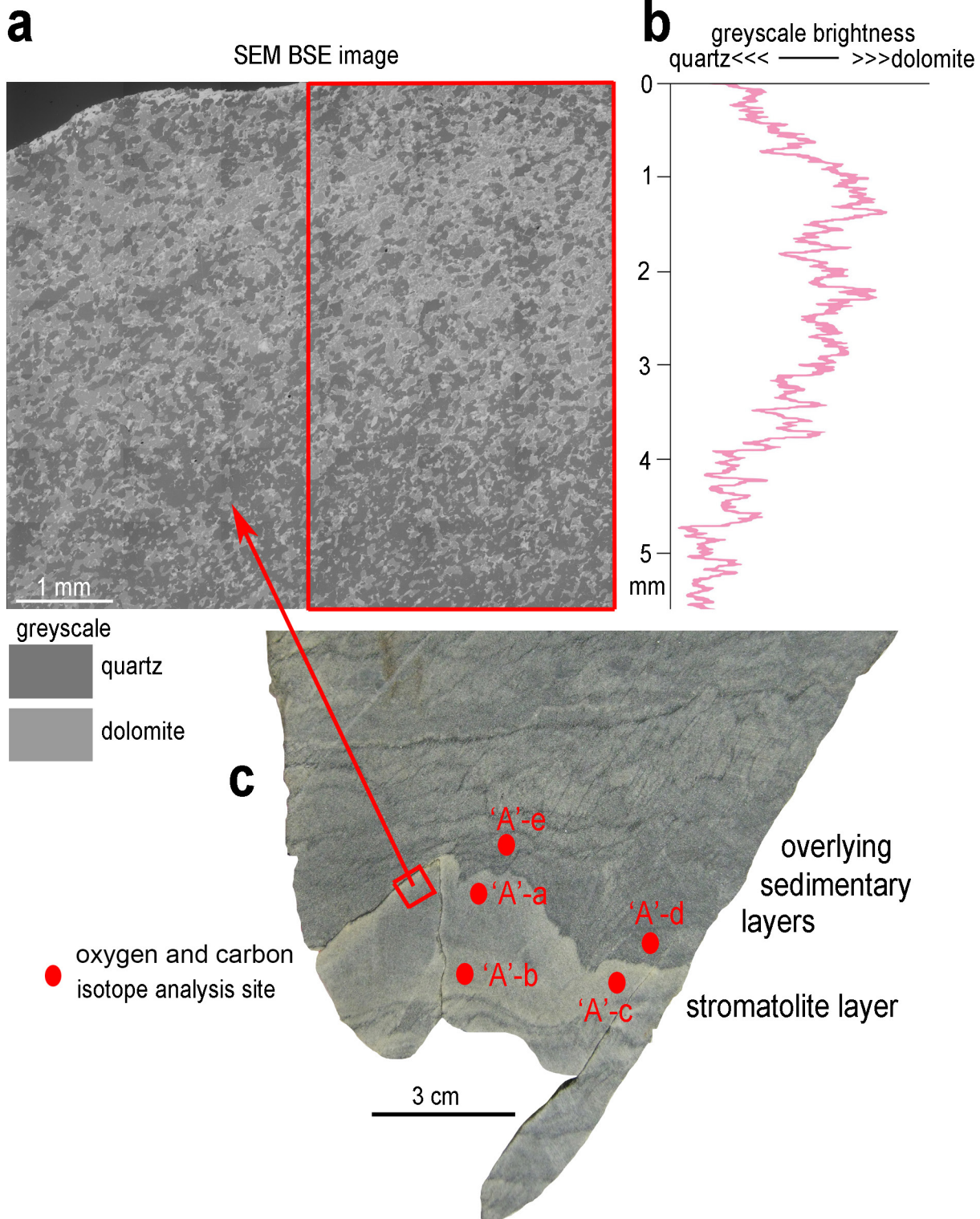
Extended Data Figure 2 | Background information on the preservation of sedimentary structures and overviews of the outcrops A and B.

a, Thin section of calc-silicate rocks ~5 m south of site A. The strain is still low, but there was ingress of an H₂O-rich fluid phase during metamorphism. Tremolite (green) is developed extensively in the left-hand side of the section, from a reaction between dolomite and quartz in the presence of the H₂O-rich fluid. The original sedimentary layering (vertical within the slide) is severely disrupted by the tremolite growth, with development of a foliation orientated from lower left to upper right.
 b, Thin section from site B where quartz and dolomite are still in

equilibrium because a CO₂-rich fluid phase was maintained during metamorphism. Fine-scale sedimentary structures are preserved (approximately horizontal across the slide). Foliation is absent. Both thin sections are shown at the same scale and are approximately 2 cm wide.

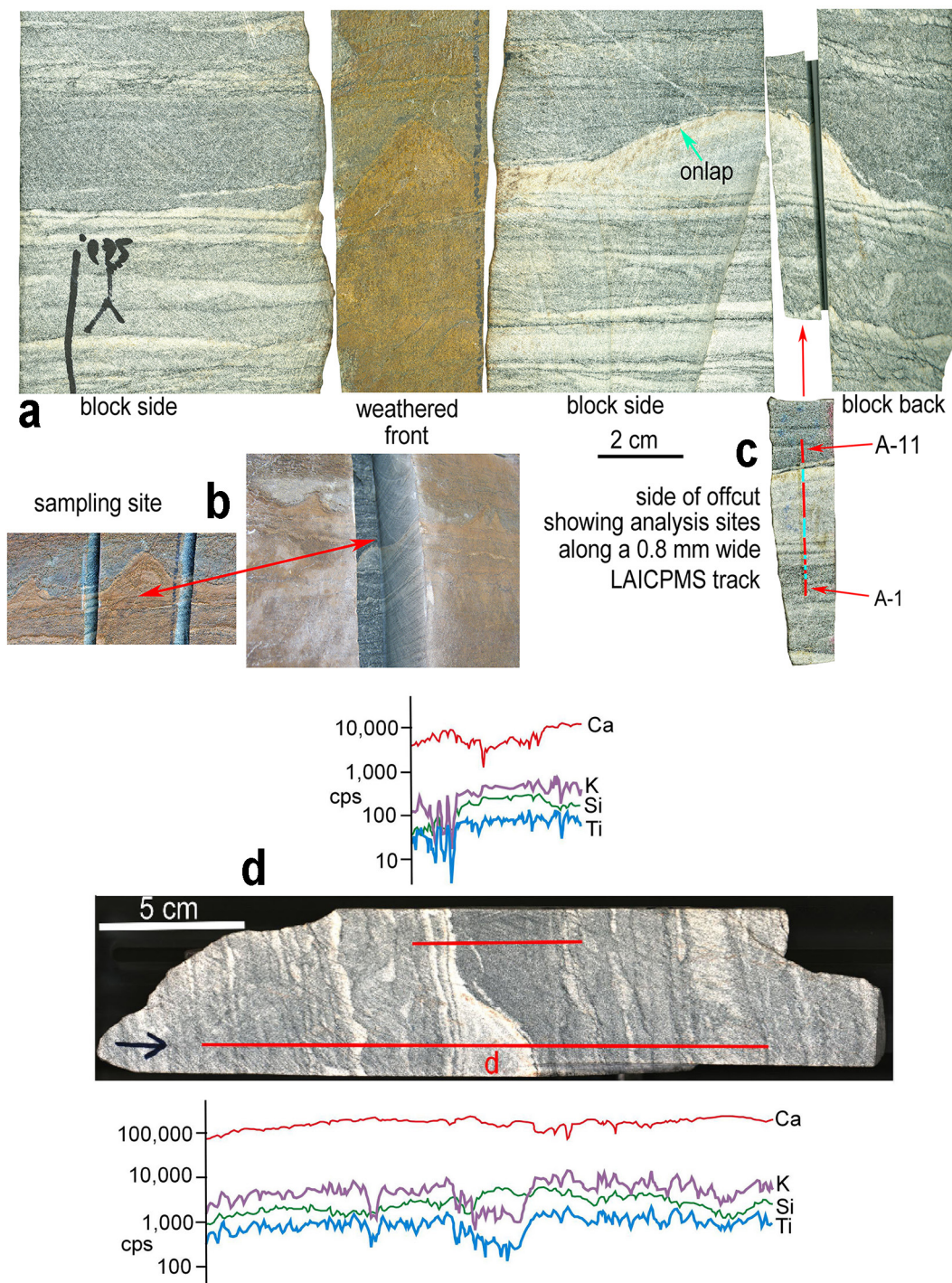
c, Overview of site A. Image inverted because outcrop is in an overturned fold limb. The red rectangle is the area shown in Fig. 1a, b. The two red parallel lines indicate the sawn block in Extended Data Fig. 4. The red arrows point to three layers with stromatolites. Field of view is 2 m.

d, Overview of site B. The detailed area shown in Fig. 2b, c is indicated by a red arrow.


Extended Data Figure 3 | Imaging of a locality A stromatolite.

Stromatolite structure from site A. **a**, SEM backscattered electron image of an area near the top of the stromatolite shown in **c**. Variation in brightness is governed by quartz (duller) versus dolomite (brighter) grains. A subtle millimetre-scale layering is visible running horizontally across the image, that is, parallel to the top of the stromatolite. This was investigated further

by examining the relative greyscales of the pixels forming the right-hand side of the image (red box in **a**). The other side of this image was not used in pixel analysis, because of the black field (beyond the edge of the scanned sample). **b**, Variation in grey scale. **c**, Sampling sites for carbonate oxygen and carbon isotope analysis (Extended Data Table 3).



Extended Data Figure 4 | Locality A stromatolite sawn blocks. Locality A sawn block. **a**, Montage of four sides of block. **b**, Sampling site pre- and post-removal of block. **c**, Location of analyses A-1 to A-11 (Extended Data Table 2). Note the onlap of this horizontal bedding to the stromatolite margin on the first block side. **d**, X-ray fluorescence ITRAX scans of a

locality A stromatolite culmination and the laterally equivalent horizon. Scans are given as relative counts per second on the relevant X-ray peak. This shows the featured stromatolite layer ('d' on the image of the rock slice) has much lower Ti and K abundances (denoting the phlogopite proxy for a lower mud content) compared with the layers above and below.

Extended Data Table 1 | Mineral analyses

	B musc-1	B phlg-1	B phlg-2	B phlg-3	B phlg-4	B phlg-5	B phlg-6	B phlg-7	B dol-1	B dol-2	B dol-3	B dol-4	B dol-5
	MU-WDS	MU-WDS	MU-WDS	MU-WDS	MU-WDS	MU-WDS							
SiO ₂	40.76	34.08	33.52	33.96	34.28	33.82	34.09	34.10	-	-	-	-	-
TiO ₂	0.05	1.11	1.08	1.06	1.09	1.08	1.08	1.04	-	-	-	-	-
Al ₂ O ₃	34.47	17.45	17.34	16.89	17.22	17.17	17.63	17.14	-	-	-	-	-
Cr ₂ O ₃	0.12	0.20	0.24	0.16	0.18	0.19	0.15	0.14	-	-	-	-	-
FeO	2.31	21.51	20.75	20.35	21.22	20.91	21.16	20.63	11.19	11.69	6.67	11.36	11.48
MnO	0.02	0.10	0.07	0.09	0.08	0.11	0.09	0.11	1.50	1.30	1.08	1.49	1.33
NiO	BDL	-	-	-	-	-							
MgO	1.04	9.87	9.88	10.14	10.04	10.06	9.82	9.99	13.22	13.14	7.37	13.20	13.36
CaO	0.04	0.05	0.06	0.20	0.10	0.15	0.26	0.30	18.94	18.78	26.01	18.65	18.84
BaO	6.14	2.12	2.31	2.05	2.03	1.91	2.13	1.87	BDL	BDL	BDL	BDL	BDL
SrO	-	-	-	-	-	-	-	BDL	0.04	0.03	0.03	0.03	0.05
Na ₂ O	0.63	0.22	0.17	0.23	0.18	0.12	0.15	0.17	-	-	-	-	-
K ₂ O	8.52	8.87	8.81	7.90	8.75	8.64	8.61	9.05	-	-	-	-	-
Cl	BDL	0.36	0.34	0.35	0.38	0.34	0.35	0.36	-	-	-	-	-
F	BDL	0.08	0.06	0.08	0.12	0.08	BDL	0.09	-	-	-	-	-
SO ₂	BDL	BDL	BDL	BDL	BDL	BDL							
Total	94.10	96.02	94.63	93.46	95.67	94.58	95.52	94.99					

	B dol-6	B dol-7	B dol-8	B cal-1*	A phlog-1	A dol-1	A dol-2	A dol-3	A dol-4	C phlog-1	C hyal-1	C hyal-2
	MU-WDS	MU-WDS	MU-WDS	MU-WDS	UW-EDS	UW-EDS	UW-EDS	UW-EDS	UW-EDS	UW-EDS	UW-EDS	UW-EDS
SiO ₂	-	-	-	-	37.02	0.17	0.04	BDL	BDL	36.7	56.96	54.11
TiO ₂	-	-	-	-	1.01	-	-	-	-	1.52	BDL	BDL
Al ₂ O ₃	-	-	-	-	18.55	BDL	BDL	0.13	0.01	17.14	20.58	21.26
Cr ₂ O ₃	-	-	-	-	-	-	-	-	-	-	-	-
FeO	11.32	11.00	3.57	1.19	20.93	21.28	19.84	25.60	21.07	23.97	0.40	0.51
MnO	1.28	1.31	1.09	0.44	0.15	2.14	2.28	2.58	2.42	0.08	0.07	BDL
NiO	-	-	-	-	-	-	-	-	-	-	-	-
MgO	13.53	12.85	2.08	0.64	10.19	24.38	25.50	21.43	26.84	8.78	0.03	0.06
CaO	18.73	18.46	31.95	22.66	0.10	52.03	52.34	50.20	49.66	0.14	0.14	0.18
BaO	BDL	BDL	BDL	BDL	2.61	BDL	BDL	BDL	BDL	2.10	11.15	13.49
SrO	0.01	BDL	0.01	BDL	-	-	-	-	-	-	-	-
Na ₂ O	-	-	-	-	0.19	-	-	-	BDL	BDL	BDL	0.98
K ₂ O	-	-	-	-	8.87	-	-	-	-	9.26	10.67	9.37
Cl	-	-	-	-	0.36	-	-	-	-	0.31	-	-
F	-	-	-	BDL	BDL	BDL	BDL	BDL	BDL	BDL	BDL	BDL
SO ₂	BDL	BDL	BDL	BDL	-	-	-	-	-	-	-	-
Total					99.98					100.00	100.00	99.96

musc, muscovite; phlg, phlogopite; dol, dolomite/ankerite; cal, calcite; hyal, hyalophane.

A, B and C refer to the sites described in the text.

MU-WDS, wave-dispersive-spectrometry analyses undertaken at Macquarie University.

UOW-EDS, examples of energy-dispersive analyses undertaken at the University of Wollongong.

BDL, below detection limit; -, not analysed.

*Calcite is a rare <10 µm reaction domain on a dolomite grain boundary.

Extended Data Table 2 | Whole-rock analyses of stromatolites and related rocks

segment #	G12/93 locality 'A' 0.8 mm wide laser ablation ICPMS traverse											Other analyses at stromatolite site	
	1 sediment below 5.5	2 sediment below 0.83	3 sediment below 1.07	4 sediment below 1.1	5 sediment below 1.23	6 sediment below 0.4	7 sediment below 6.29	8 within stromat. 6.57	9 within stromat. 9	10 within stromat. 4	11 sediment above 8	G11/63	G11/72
length (mm)												dolostone	breccia
oxides wt%													
SiO ₂	18.70	33.75	14.56	36.86	14.22	72.58	15.35	30.92	38.03	16.12	38.25		
Al ₂ O ₃	3.68	8.15	4.97	4.76	1.15	2.77	1.77	1.15	1.21	0.74	4.51		
FeCO ₃	9.74	7.73	10.76	8.60	11.39	2.98	11.66	9.74	9.31	13.11	8.31		
MgCO ₃	13.57	7.48	14.43	10.09	17.33	3.98	17.92	15.39	12.07	17.81	9.56		
CaCO ₃	49.33	23.37	48.63	28.18	58.92	14.56	56.90	44.81	38.01	58.19	29.22		
Total	85.27	72.74	82.59	79.90	91.63	93.88	91.95	92.27	89.32	92.86	81.54		
ppm													
Li	12.6	29.4	18.3	22.1	4.8	4.3	6.0	3.7	3.1	2.9	14.4		
P	25.9	8.2	5.2	8.0	806.6	560.6	21.2	72.5	85.9	104.2	17.9		
Ti	568	1330	781	953	211	120	252	142	116	104	619		
V	44.5	101.7	61.3	62.5	14.6	28.4	21.6	12.5	12.2	8.8	52.6		
Cr	323	917	575	627	124	126	147	40	26	81	437	210	140
Co	15.6	19.2	18.5	17.5	14.9	4.0	14.5	10.9	9.2	12.6	11.4		
Ni	47.1	91.5	63.1	72.3	32.0	12.3	33.3	23.6	19.0	24.1	37.3		
Zn	35.8	48.0	42.0	42.8	33.3	12.8	32.5	26.1	23.1	28.6	31.0		
Ga	3.02	7.05	4.17	4.13	0.99	2.41	1.48	0.89	0.92	0.60	3.71		
Rb	31.9	75.8	44.1	53.3	12.1	12.2	14.4	8.8	7.4	6.5	37.1	22.4	17
Sr	46.4	29.5	47.0	27.0	53.5	16.0	52.1	41.2	34.8	53.5	30.9	63.4	17.5
Y	8.27	10.82	8.61	4.59	8.16	4.88	7.05	5.09	4.51	9.52	8.31	6.6	8
Zr	10.4	28.9	11.0	7.0	3.6	8.4	3.8	3.8	5.2	6.0	16.5	9	14
Nb	0.29	0.68	0.41	0.46	0.10	0.13	0.14	0.09	0.08	0.06	0.37	0.5	0.6
Ba	1843	3862	2453	2069	525	1661	942	597	886	409	2350	1295	9640
La	2.72	8.47	2.93	1.59	1.09	1.67	2.21	1.24	0.94	2.60	2.58	2.2	2.4
Ce	4.49	13.80	4.76	2.76	1.78	2.80	3.73	2.18	1.71	4.37	4.22	3.4	3.5
Pr	0.54	1.63	0.57	0.33	0.22	0.34	0.46	0.28	0.22	0.53	0.50	0.41	0.39
Nd	2.35	7.03	2.44	1.41	1.04	1.34	2.09	1.26	1.03	2.35	2.07	1.6	1.4
Sm	0.61	1.60	0.63	0.38	0.34	0.36	0.58	0.37	0.32	0.64	0.51	0.4	0.29
Eu	0.34	0.66	0.33	0.22	0.25	0.30	0.33	0.25	0.21	0.34	0.26	0.46	0.15
Gd	0.83	1.71	0.84	0.51	0.65	0.50	0.80	0.56	0.48	0.94	0.67	0.66	0.67
Tb	0.14	0.24	0.15	0.09	0.13	0.09	0.14	0.10	0.09	0.17	0.12	0.11	0.12
Dy	1.00	1.47	1.01	0.57	0.95	0.62	0.91	0.67	0.60	1.15	0.90	0.66	0.73
Ho	0.23	0.30	0.24	0.13	0.23	0.14	0.21	0.16	0.14	0.27	0.23	0.17	0.19
Er	0.72	0.87	0.74	0.39	0.68	0.39	0.60	0.46	0.41	0.82	0.73	0.46	0.53
Tm	0.11	0.13	0.11	0.06	0.10	0.06	0.09	0.07	0.06	0.12	0.12	0.07	0.08
Yb	0.73	0.89	0.77	0.41	0.64	0.39	0.59	0.44	0.39	0.83	0.82	0.46	0.49
Lu	0.12	0.12	0.07	0.10	0.07	0.10	0.08	0.07	0.07	0.13	0.13	0.09	0.08
Hf	0.33	0.36	0.24	0.13	0.33	0.13	0.14	0.00	0.17	0.13	0.54	0.3	0.5
Pb	2.26	2.25	1.83	2.18	1.57	2.10	2.02	18.62	1.96	2.28	2.29		
Th	0.22	1.01	0.22	0.11	0.10	0.23	0.11	0.00	0.08	0.18	0.27	0.13	0.25
U	0.07	0.11	0.06	0.04	0.07	0.05	0.05	0.01	0.06	0.09	0.10	0.06	0.1

Major element composition calculated assuming Fe, Mg and Ca are largely present as carbonates and Si and Al are oxides.

This is supported by the strong positive correlation of Ca with Fe and Mg and negative correlations with Si and Al.

Extended Data Table 3 | Carbon and oxygen isotopic analysis of a site A stromatolite

	$\delta^{13}\text{C}_{\text{VPDB}}$	$\delta^{18}\text{O}_{\text{VSMOW}}\text{raw}$	$\delta^{18}\text{O}_{\text{VSMOW}}\text{corr}$	$\delta^{18}\text{O}_{\text{VPDB}}\text{approx}^*$
A-a	1.41	19.38	18.46	-12.07
	1.31	19.39	18.47	-12.06
A-b	1.44	19.37	18.45	-12.08
	1.48	19.26	18.34	-12.19
	1.47	19.33	18.41	-12.12
A-c	1.41	19.34	18.42	-12.11
	1.35	19.20	18.28	-12.25
	1.46	19.25	18.33	-12.20
A-d	1.20	19.23	18.31	-12.22
	1.22	19.17	18.25	-12.28
A-e	1.30	19.31	18.39	-12.14
	1.35	19.25	18.33	-12.20

*The VPDB $\delta^{18}\text{O}$ scale strictly only applies to calcite, not to other carbonates. Accordingly, the data column labelled $\delta^{18}\text{O}_{\text{VPDB}}\text{approx}$ refers to the conversion from the corrected $\delta^{18}\text{O}_{\text{VSMOW}}$ values using $\delta^{18}\text{O}_{\text{VPDB}} = 0.97002(\delta^{18}\text{O}_{\text{VSMOW}}) - 29.98$.

See Extended Data Fig. 3c for location of analyses.

The replicate analyses refer to separate CO_2 extractions of powdered sample.